Article

Journal of the Brazilian Chemical Society

https://dx.doi.org/10.21577/0103-5053.20240121

J. Braz. Chem. Soc. **2024**, *35*, 12, e-20240121, 1-12

Revisiting the Synthesis and Characterization of Hybrid Nanomaterial Constituted by Folate Intercalated into M^{2+}/Al^{3+} (M^{2+} = Mg^{2+} and Zn^{2+}) Layered Double Hydroxide

Vagner R. Magri,[a] *Caroline S. de Matos,*[a] *Michele A. Rocha,*[a] *Christine Taviot-Gueho*[b,c] *and Vera R. L. Constantino*[*,a]

[a]*Departamento de Química Fundamental, Instituto de Química, Universidade de São Paulo, 05513-970 São Paulo-SP, Brazil*

[b]*Université Clermont Auvergne, Université Blaise Pascal, Institut de Chimie de Clermont-Ferrand, BP 10448, F-63000 Clermont-Ferrand, France*

[c]*CNRS, UMR 6296, ICCF, F-63178 Aubiere, France*

Intercalation of deprotonated folic acid (FA; vitamin B9) is of great interest for nutraceutical and cosmeceutical purposes. Although some studies have already reported the intercalation of divalent ($HFol^{2-}$) or trivalent (Fol^{3-}) folate anions into layered double hydroxides (LDH), the structure, spectroscopic, and thermal behavior of such hybrid materials still need to be better understood. This work revisited the synthesis of LDH constituted by M^{2+}/Al^{3+} (M^{2+} = Mg or Zn) intercalated with $HFol^{2-}$ or Fol^{3-}. Insights concerning how the physicochemical properties of the materials are tuneable according to the synthetic approach (slow or fast coprecipitation) and pH value (7.5 or 9.0/9.5) of synthesis were pointed out. Materials synthesized at pH above 9.0 (Fol^{3-}) presented larger particles and lower loading capacity than the ones synthesized at pH 7.5 ($HFol^{2-}$). The fast coprecipitation approach led to the formation of materials with smaller particles. This work could address the following research concerning LDH-FA applications.

Keywords: layered double hydroxide (LDH), folic acid, vitamin B9, hybrid materials, intercalation compounds

Introduction

A diversified number of organic-inorganic hybrid materials constituted by layered double hydroxides (LDH) intercalated with bioactive anionic organic species have been synthesized since the early 2000s, focusing on developing drug delivery and theragnostic systems.[1-5] LDH structure (Figure 1a) is constituted of hydroxide ions coordinated to metal cations in the center of octahedrons ($M(OH)_6$). The octahedrons are interconnected by edges, forming a layered structure similar to the brucite mineral ($Mg(OH)_2$).[6] Isomorphic substitution of bivalent by trivalent metal cations in the brucite-like layers confers an equivalent positive residual charge ($[M^{3+}] = [q^+]$) to the structure. Electroneutrality is reached by intercalating hydrated-exchangeable anions into the LDH interlayer region. Typically, LDH are represented by the general formula $[M^{2+}_{(1-x)}M^{3+}_x(OH)_2]^{x+}[(A^{n-})_{x/n}{\cdot}mH_2O]$, where M^{2+} is a divalent metal cation (Mg^{2+}, Zn^{2+}, Ni^{2+}, Co^{2+}, Cu^{2+}, Fe^{2+}, etc.) and M^{3+} is a trivalent one (Al^{3+}, Ga^{3+}, Co^{3+}, Fe^{3+}, etc.). A^{n-} represents the anion, which can be inorganic (CO_3^{2-}, Cl^-, NO_3^-, etc.), organic, polymeric or a coordination compound. The LDH composition is abbreviated $M^{2+}_RAl^{3+}$-A (where R = $[M^{2+}]/[M^{3+}]$ molar ratio). The x value of the general formula represents the $[M^{3+}]/([M^{2+}] + [M^{3+}])$ molar fraction, which generally varies between $0.2 \leq x \leq 0.33$ (or R-value between 4 and 2).[1-3,6,7]

The LDH structure can improve the chemical stability of the loaded anionic species and promote its sustained release, which can avoid low drug bioavailability and side effects.[1-3] Compared to other drug delivery systems, LDH presents advantages, such as (*i*) versatility in terms of composition and physicochemical properties, (*ii*) synthesis by soft-chemical methods, (*iii*) low cost; (i*v*) disruption in acid media (pH-responsive material); (*v*) anionic exchange capacity; and (*vi*) *in vitro* and *in vivo* biocompatibility for some chemical compositions.[1-3,6,7]

*e-mail: vrlconst@iq.usp.br
Editor handled this article: Ítalo O. Mazali (Guest)
This work is dedicated to Prof Dr Oswaldo L. Alves, a pioneer and enthusiastic researcher in solid-state chemistry.

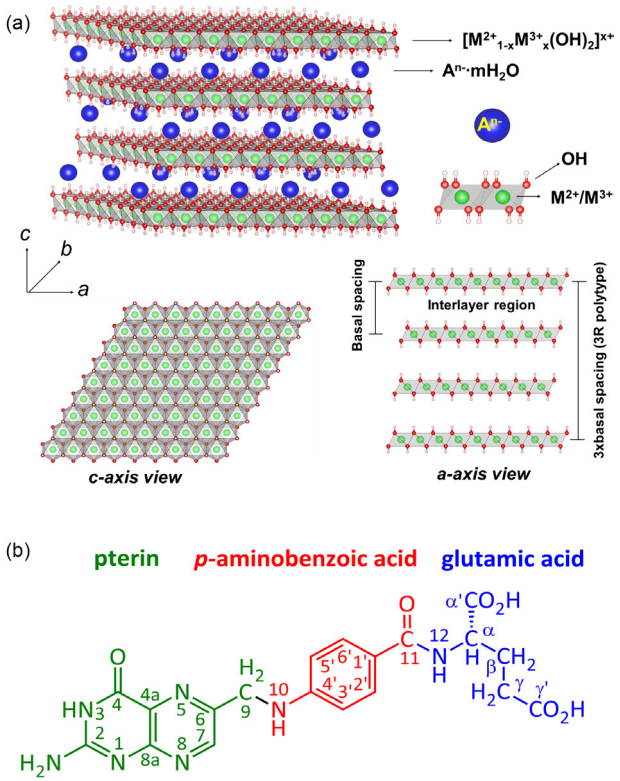

Figure 1. Schematic representation of the LDH structure with rhombohedral symmetry (3R1 three-layer polytype) in R-3m space group (a) and molecular structure of folic acid (b).

Due to its outstanding bioactivity, folic acid (FA) has attracted significant interest in being administrated through drug delivery systems.[8-10] FA is the synthetic analogue of micronutrient groups called folates, known as vitamin B9. Its molecular structure (Figure 1b) is constituted by three chemical moieties: pterin (PT), *p*-aminobenzoic acid (*p*-ABA) and L-glutamic acid (Glu). The FA presents antioxidant, cellular redox-balance and cell-proliferative (deoxiribonucleic acid (DNA) and ribonucleic acid (RNA) synthesis and repair) properties.[8-10] It is used as a food fortifier or supplement to avoid anaemia, birth neural tube defects, to control homocysteine levels (related to endothelial dysfunction), and dementia, for instance.[8-11] Furthermore, FA-targeted drugs and nanoparticles can be applied in oncology[12] or rheumatoid arthritis[13] treatment because of the targeting activity of folates on cancerous and macrophage cells, respectively. For instance, LDH surface-modified with folate systems are internalized through active targeting by cancerous cells or preferentially accumulate in tumour in a higher extension than pristine material (passive targeting).[14,15]

Hybrid materials constituted of divalent ($HFol^{2-}$) or trivalent (Fol^{3-}) folic acid anionic species (folates) were also evaluated as nutraceutical and cosmeceutical carriers.[16-22] Table S1 (Supplementary Information (SI) section) summarizes the studies in the literature about the synthetic methods and characterization of such hybrid materials. Significant advantages regarding the intercalation of folates in LDH structure were described,[16-23] as detailed and discussed in the SI section. However, most of the work has yet to successfully obtain well-crystalized LDH-FA materials with phase purity and a high amount of intercalated folate, which are required for meaningful physical-chemical characterization, regulation of the drug release and safety (no harmful or fortuitous impurities and less carrier material). In this work, hybrid nanomaterial constituted by folate anionic species ($HFol^{2-}$ and Fol^{3-}) intercalated into the M^{2+}/Al^{3+}-LDH (M^{2+} = Mg^{2+} and Zn^{2+}) materials were synthesized by two approaches comprising slow and fast coprecipitation. The main goal was to obtain materials with phase purity to afford an assertive structural, thermal, and spectroscopic characterization of such a folate nanocarrier. The influence of pH value on the preparation of the materials was also investigated. The structure and chemical composition of LDH-FA nanohybrids were evaluated by X-ray diffractometry (XRD), vibrational spectroscopy (infrared and Raman), scanning electron microscopy (SEM), transmission electron microscopy (TEM), chemical analysis (metal content and carbon, hydrogen, and nitrogen (CHN) percentage), and simultaneous thermal analysis coupled to mass spectrometry (TGA-DSC-MS). This work can drive the subsequent research regarding the synthesis, characterization, and application of LDH-FA hybrid materials. Furthermore, the fast coprecipitation approach reported here could be extended to intercalate other organic anions since it has not been much explored in the literature.

Experimental

Chemicals

Magnesium chloride hexahydrate ($MgCl_2\cdot6H_2O$; 99%) was purchased from Merck (Darmstadt, Germany), and HCl (37%; analytical grade) was supplied by LabSynth (São Paulo, Brazil). Folic acid di-hydrated (FA; $C_{19}H_{19}N_7O_6\cdot2H_2O$; ≥ 97%), anhydrous zinc chloride ($ZnCl_2$; ≥ 98%), aluminium chloride hexahydrate ($AlCl_3\cdot6H_2O$; 99%) and sodium hydroxide (NaOH; ≥ 98%) were acquired from Sigma-Aldrich (St. Louis, USA). The reagents were used without any further purification. Deionized water (18 MΩ cm) purified from the Milli-Q Millipore Co. system (Bedford, USA) was used in all experiments.

Synthesis of the hybrid materials

Hybrid materials were synthesized by the coprecipitation method using two approaches: (*i*) slow coprecipitation with

the control of the pH value (constant pH) and (*ii*) fast coprecipitation without the control of the pH value. The obtained materials are undermentioned as LDH-FA or $M^{2+}{}_R$- Al-A-S,F, where M^{2+} is the divalent cation (Mg^{2+} or Zn^{2+}), R represent the M^{2+}/Al^{3+} nominal molar ratio equal two, A is the anion ($HFol^{2-}$ or Fol^{3-}) and S and F means slow and fast coprecipitation, respectively. It was considered that the FA molecule possesses two carboxylic acids and one amidic group, marked in Figure 1b as Cα'OOH (pK_{a2} = 3.38), Cγ'OOH (pK_{a2} = 4.83) and N3–H (pK_{a3} = 7.85).[24] Accordingly, the anionic predominant species is $HFol^{2-}$ at pH 7.5, while above pH 9.0, the dominant species is Fol^{3-} (Figure S1, SI section).

Slow coprecipitation method

Zn_2Al-HFol-S, Zn_2Al-Fol-S and Mg_2Al-Fol-S hybrid materials were synthesized based on previous work,[25-27] with some modifications. Divalent folate anion ($HFol^{2-}$) intercalation into Zn_2Al-LDH was performed at a constant pH value under the N_2 atmosphere. In detail, an aqueous solution containing approximately 16.7 mmol of $ZnCl_2$ and 8.33 mmol of $AlCl_3{\cdot}6H_2O$ (ca. 0.1 mol L^{-1}) was dropwise in an aqueous solution containing 8.33 mmol of FA at pH value previously adjusted to 7.5 by the addition of NaOH aqueous solution (ca. 0.2 mol L^{-1}). The addition was carried out at an approximate rate of 0.5 mL min^{-1}, under vigorous mechanical stirring and at 60 ± 5 °C. The pH value of the medium was maintained constant by the simultaneous addition of the NaOH solution. After adding the metal cation solution, the system was kept at the same conditions (i.e., 60 °C, mechanical stirring and N_2 atmosphere) for 24 h. The precipitated yellow solid was isolated and rinsed with deionized water by centrifugation (17 000 rpm for 5 min at 25 °C) until a negative chloride ion test (monitored with $AgNO_3$ solution). The slurry was then dispersed in water, frozen under immersion in liquid nitrogen (–196 °C) and freeze-dried for three days in a Thermo Savant ModulyoD (Thermo Fisher Scientific; Waltham, USA) equipment (200 mPa and –50 ºC). The obtained solid was named Zn_2Al-HFol-S. The intercalation of trivalent folate anion (Fol^{3-}) into Mg_2Al-LDH was carried out by the same synthetic method reported for Zn_2Al-LDH but at a pH value of 9.5 and using solutions containing 20.0 mmol of $MgCl_2{\cdot}6H_2O$ and 10.0 mmol of $AlCl_3{\cdot}6H_2O$ (ca. 0.1 mol L^{-1}) and 10.0 mmol of FA. The isolated solid was named Mg_2Al-Fol-S. For comparison purposes, Zn_2Al-LDH was also synthesized at a pH value of 9.0, using 3.33 mmol of $ZnCl_2$, 1.67 mmol of $AlCl_3{\cdot}6H_2O$ (ca. 0.1 mol L^{-1}) and 1.67 mmol of FA. The obtained solid was abbreviated Zn_2Al-Fol-S.

Fast coprecipitation method

Two solutions were initially prepared for the fast coprecipitation approach. Solution A was obtained by dissolving 3.33 mmol of $MgCl_2{\cdot}6H_2O$ (or $ZnCl_2$) and 1.67 mmol of $AlCl_3{\cdot}6H_2O$ in 50 mL of water. Solution B was prepared by dissolving 1.12 mmol of FA in 100 mL of an aqueous solution containing 0.133 mol L^{-1} NaOH (or 0.122 mol L^{-1} for Zn_2Al-HFol-F). After that, solution A was added (approximately 300 mL min^{-1}) in solution B under vigorous stirring, reaching a final [FA]/[Al^{3+}] molar ratio equal to 0.67. Then, the pH value of the media was adjusted to 7.5 (for Zn_2Al-HFol-F) or 9.5 (for Zn_2Al-Fol-F and Mg_2Al-Fol-F) by adding standard HCl (0.1 mol L^{-1}) or NaOH (0.2 mol L^{-1}) solution. The pH value adjustment was made to ensure the intercalation of desired folate anionic species, i.e., $HFol^{2-}$ (pH 7.5) or Fol^{3-} (pH 9.5). Table S2 (SI section) shows the pH value variation of the synthesis media during the process. The system was kept at 60 ± 5 °C under N_2 atmosphere for 24 h. Finally, as mentioned above, the obtained materials were rinsed three times with water and freeze-dried.

To improve the crystallinity of Zn_2Al-HFol-F, the material was submitted to an additional hydrothermal ageing step. After 24 h at 60 °C, the sample was isolated by centrifugation, rinsed twice, resuspended manually in water (approximately 50 mL *per* 1 mmol of Al^{3+} used in the synthesis) and transferred to a stainless-steel reactor containing a Teflon cup (100 mL volume). The reactor was placed inside an oven (heating rate of ca. 4 °C min^{-1}) and heated for 1 h after reaching 150 °C. Next, the system was cooled naturally to room temperature. Finally, the sample was isolated by centrifugation, washed once with water and freeze-dried.

Ion-exchange method

For comparison, the Zn_2Al-HFol material was also prepared using the ion-exchange method. The Zn_2Al-NO_3 precursor was prepared by coprecipitation method as follows: 10 mL of an aqueous solution containing 167.0 mmol L^{-1} of $Zn(NO_3)_2{\cdot}6H_2O$ and 83.0 mmol L^{-1} of $Al(NO_3)_3{\cdot}9H_2O$ was added dropwise (0.11 mL min^{-1}) in 100 mL of water that had its pH value previously adjusted to 7.5 by the addition of 0.5 mol L^{-1} NaOH solution. During the salt addition, the pH value was maintained constant by the simultaneous addition of the NaOH solution. After that, the white slurry was isolated by centrifugation and washed once with water. Then, the slurry of freshly prepared Zn_2Al-NO_3 was manually dispersed in 10 mL of water and gently transferred to 40 mL of FA solution (28 mmol L^{-1}; pH previously adjusted to 7.5), reaching a [FA]/[Al^{3+}] molar ratio of 0.67. The system was kept under

stirring and N_2 atmosphere at room temperature for 24 h. Finally, the orange solid was isolated, washed three times with water, dried overnight in an oven at 60 °C, and then ground in a mortar.

Physical measurements

XRD patterns of powdered samples were recorded in a Bruker D8 DISCOVER (Billerica, USA) diffractometer (40 kV and 30 mA) with Cu Kα radiation (λ = 0.15418 nm) source and collected in the 3-70° (2θ) range, with steps of 0.05° (2θ) and scan speed of 0.05° for 3 s. Fourier transform infrared (FTIR) spectra of powdered samples were recorded on a Bruker Alpha (Billerica, USA) spectrometer (DTGS detector and KBr optics) using a single bounce attenuated total diffuse reflectance (ATR) mode with a diamond crystal in the 4000-400 cm^{-1} spectral range, 4 cm^{-1} of resolution and accumulating 512 scans. Fourier transform Raman (FT-Raman) spectra were recorded on Bruker (Billerica, USA) instrument, MultiRam model, equipped with Ge detector (cooled by liquid nitrogen) using excitation radiation of 1064 nm (Nd^{3+}/YAG laser) and 100-200 mW of power on the sample, in the 3500-150 cm^{-1} spectral range, with 4 cm^{-1} of resolution and accumulating 1024 scans. Simultaneous thermogravimetry and differential scanning calorimetry analysis (TGA/DTG-DSC) coupled to mass spectrometry (MS) were conducted on a Netzsch (Selb, Germany) thermoanalyzer, model STA 409 PC Luxx, connected to a QMS 403C Aëolos MSD mass spectrometer. The analysis was performed up to 1000 °C under an air atmosphere with a flow rate of 50 mL min^{-1}, a heating rate of 10 °C min^{-1}, and an alumina crucible. Carbon, hydrogen, and nitrogen elemental analyses were performed in a PerkinElmer model 2400 (Waltham, USA) analyzer. Magnesium, zinc, and aluminium metal contents were determined by inductively coupled plasma optical emission spectroscopy (ICP OES) on a Spectro Arcos (Kleve, Germany) spectrometer. Both analyses were carried out in triplicate at the Central Analítica of the Instituto de Química-Universidade de São Paulo (CA-IQUSP). The percentage of hydration water and residual mass was obtained by thermal analysis. SEM images were registered in a JEOL (Tokyo, Japan) microscope, model JSM-6610LV, operating at 10 kV and using a secondary electron imaging (SEI) detector. Before the analysis, powdered samples were deposited on aluminium stubs covered with carbon tape and then coated with a thin layer of gold using a Desk V magnetron sputter (Denton Vacuum; Moorestown, USA). TEM images were acquired on a Hitachi H-7650 (Tokyo, Japan) microscope operating with an accelerating voltage of 80 kV. The sample was prepared by suspending the material in ethanol (1 mg mL^{-1}) under ultrasound for 0.5 h. Then, the suspension was dropped onto a copper grid (150 mesh) coated with Formvar/carbon film.

Results and Discussion

XRD characterization

The XRD patterns of hybrid LDH-FA samples obtained by slow or fast coprecipitation methods were typical of the LDH phase (Figures 2a and 2b).[25-27] The diffraction peaks were indexed considering a hexagonal cell of rhombohedral symmetry (3R polytype) in the R-3m space group. No other crystalline phase was identified, indicating the obtention of materials with phase purity. The interplanar spacings and lattice parameters calculated from XRD data are summarized in Tables S3-S4 (SI section). The intercalation of folate anions in the interlayer space of LDH was confirmed by the displacement of the peaks attributed to the family of 00*l* planes (related to the basal spacing – d_{00l}; Figures 2a and 2b) to lower 2θ values in comparison with LDH-Cl counterpart reported in the literature.[25,26] The overlap of peaks 110 and 113 (Figures 2a and 2b) is also consistent with the increase of the interlayer and indicates that it has not formed a non-folate intercalated LDH phase.[25-27]

The quality of the present XRD data (Figure 2), together with the chemical analysis of the samples discussed below, leaves no doubt about folate intercalation and the purity of the samples. The basal spacing was tunable according to the pH value of the synthesis: materials synthesized at pH 7.5 (Zn_2Al-HFol-S and Zn_2Al-HFol-F) presented a mean basal spacing of 2.50 nm. In contrast, for the ones prepared at pH above 9.0 (Mg_2Al-Fol-S, Mg_2Al-Fol-F, Zn_2Al-Fol-S and Zn_2Al-Fol-F), the basal spacing decreased to around 1.63 nm. The species of folate anion ($HFol^{2-}$ or Fol^{3-}) depends on the pH value of the media (Figure S1). Accordingly, distinct preferential arrangements of $HFol^{2-}$ and Fol^{3-} in the interlayer space of LDH matrices were expected, considering that the layer charge densities were the same for the isolated hybrids (the lattice parameters reported in Tables S3-S4, SI section, were compatible with M^{2+}/M^{3+} molar ratio equal 2).[25-27] Results from the literature[16,21] related basal spacings varying around 1.60 and 1.82 nm for Mg_2Al-LDH materials synthesized by the coprecipitation method at pH 10, in which Fol^{3-} is the dominant species (Figure S1). In this work, the result agreed with the 1.60 nm value previously reported by Qin *et al.*[16] The works described in the literature (Table S1) concerning the ion exchange method used the precursors of composition Zn_RAl-LDH (R = 2-2.5) and pH 7-8.[20,23] The

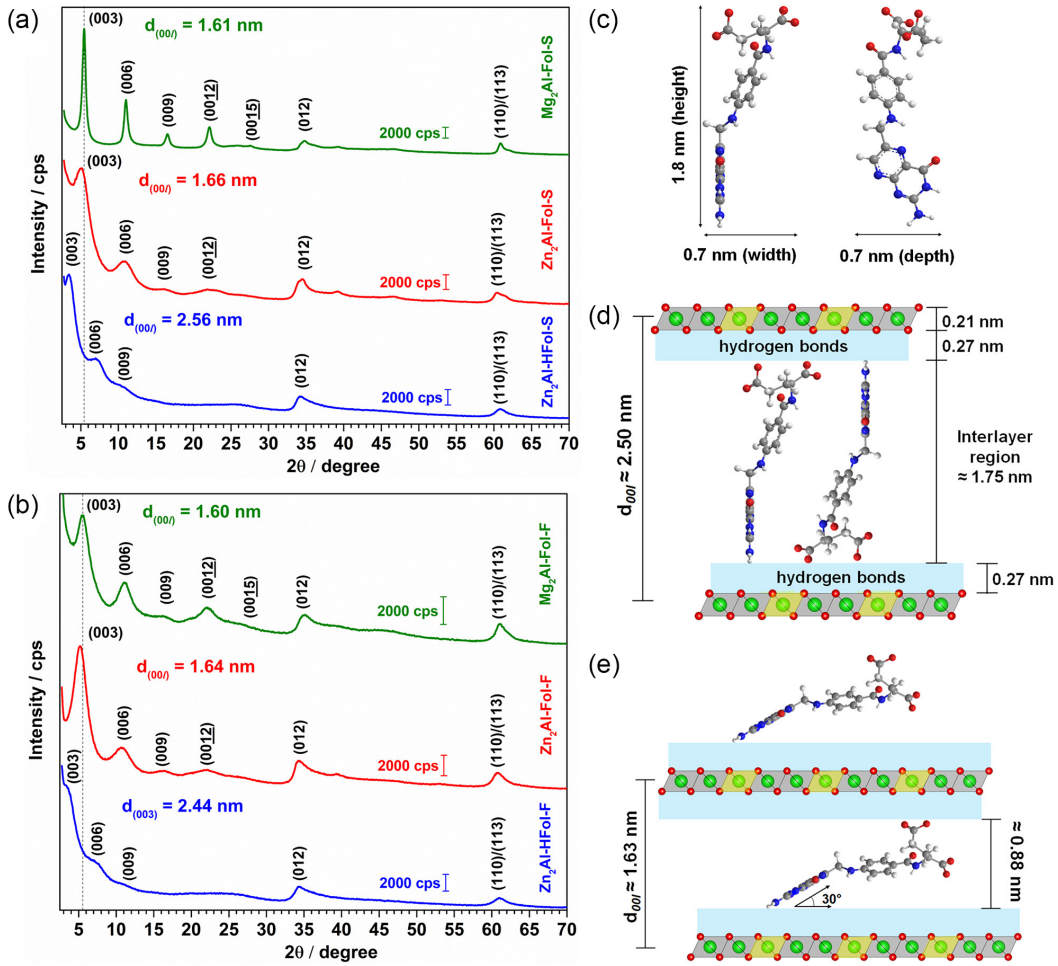

Figure 2. XRD patterns of powdered samples obtained by slow coprecipitation (a) and fast coprecipitation (b); folate dimensions estimated by Chem3D Pro software[28] (c); arrangement proposed for $HFol^{2-}$ intercalated into Zn_2Al-HFol-S and Zn_2Al-HFol-F samples (d); arrangement proposed for Fol^{3-} intercalated into Mg_2Al-Fol-S, Mg_2Al-Fol-F, Zn_2Al-Fol-S and Zn_2Al-Fol-F samples (e). The arrangement of folate anions was proposed, considering the arrangement of molecules in the crystal structure of dihydrate FA resolved by Kaduk *et al.*[29]

basal spacings noticed were around 1.60 nm, a significantly lower value than the ones observed in this work for Zn_2Al-HFol-S and Zn_2Al-HFol-F (Figure 2 and Tables S3-S4). Therefore, the synthetic method can also influence the arrangement of folate anions inside the interlayer space because the level of ion-exchanged anions can be low, generating materials with co-intercalated anions.[30] A higher amount of folate was observed using the coprecipitation than the ion-exchange method for Mg_2Al-LDH systems.[16,21] In the ion exchange approach, the organic species, usually more prominent than the anions in the precursor LDH, can take a tilted orientation between the layers, decreasing the basal spacing.[30] The XRD data of Zn_2Al-HFol prepared by ion-exchange method (starting from Zn_2Al-NO_3, as reported in the literature[20,22,23]) confirmed this hypothesis (Figure S2a).

The proposal of an arrangement for folate anions inside the interlayer space is not straightforward because folate structure presents a high degree of freedom, making many folded conformations possible.[31] However, organic anions intercalated in LDH maintain a conformation similar to their acidic form in solid crystal[26,32] because the lowest energy packing can be achieved.[32] Such a proposal was reported for sulindac[26] and mefenamic[32] anions from the correlation of theoretical results of a one-dimensional electron density plot (applied to XRD results of LDH-A) and density functional theory (DFT) calculations of their acidic form. Kaduk *et al.*[29] resolved the dihydrate FA crystal structure by Rietveld refinement and geometry optimization by DFT. Glu moieties are bent concerning the *p*-ABA and PT ones, which are tilted about each other due to hydrogen bonds.[29] The unit cell *c*-axis was 3.24 nm, and the d_{002} value, related to the height dimension of one molecule, was ca. 1.60 nm.[29] The dimensions of folate anions were estimated in this work to be 1.8 × 0.7 × 0.7 nm (Figure 2c) using Chem3D Pro software.[28] The difference in the estimated folate arrangement was in the Glu moiety, which was not folded as in FA crystal.

Considering the LDH layer thickness (0.21 nm) and the hydrogen-bond distances between LDH and intercalated anions (2 × 0.27 nm), the interlayer distance occupied by the guest was estimated to be around 1.89 nm (Zn_2Al-HFol-S and Zn_2Al-HFol-F) and 0.88 nm (Mg_2Al-Fol-S, Mg_2Al-Fol-F, Zn_2Al-Fol-S and Zn_2Al-Fol-F), as represented in Figures 2d and 2e. Considering the good match between the estimated height dimension of the $HFol^{2-}$ (1.8 nm) and the interlayer room available (approximately 1.75 nm) in Zn_2Al-HFol-S and Zn_2Al-HFol-F materials, a monolayer arrangement of anion species could be proposed, in which Glu moiety is parallel to the LDH layer. In contrast, the PT moiety is perpendicular to the layer (Figure 2d). Considering the gallery available (approximately 0.88 nm) for materials synthesized at pH value 9.0, Fol^{3-} anions could be intercalated in a monolayer and tilted at an estimated angle of around 30° along the crystallographic c-axis, in which Glu moiety is perpendicular (Figure 2e). Some studies[16-19] also proposed that Fol^{3-} was tilted along the c-axis, but the tilt angle estimated varied between 60 and 70°. However, the unfolded anion conformation was considered, and hydrogen bonds between guest and host were disregarded. Such changes in the anion array according to the pH of synthesis can be attributed to the fact that Fol^{3-} also has a charge in the PT group. Then, the tendency of folate anion to be arranged in a tilted array pattern to maximize the interactions between the anion and the oppositely charged layer is plausible.

Considering an ideal Al^{3+} distribution in the intralayer, the surface area occupied by a charge in the LDH structure is around 0.25 nm^2/q^+ (or 0.50 nm^2/q^+ if both layer sides are considered).[33] By assuming a parallelepiped of about 1.8 nm × 0.7 nm × 0.7 nm enclosing the molecular shape of folic acid molecule (see Figure 2c), one can calculate two different surface areas *per* unit charge for each folate anion depending on the orientation concerning the hydroxide layers. The estimated area occupied by $HFol^{2-}$ in a perpendicular orientation is 0.49 nm^2 (0.7 × 0.7 nm), corresponding to a charge density of ca. 0.25 nm^2/q^-, which is quite the same as the charge density of LDH. Therefore, charge balancing can be obtained from close packing and a perpendicular orientation of $HFol^{2-}$ anions concerning the LDH layers. Otherwise, the lower interlayer distance measured for intercalated Fol^{3-} species (in Mg_2Al-Fol-S, Mg_2Al-Fol-F, Zn_2Al-Fol-S and Zn_2Al-Fol-F) is consistent with a titled orientation with an inclination angle of about 30° (Figure 2e). Thus, the estimated projected area of the anion to the layer was around 1.1 nm^2, corresponding to about 0.37 nm^2/q^-. This value is higher than the LDH layer charge density. Hence, the anions should be arranged away from each other in this case, and the co-intercalation of a small chloride anion is required to reach the electroneutrality of the material. Figure S3a (SI section) presents a proposal for the neutralization of 10 positive electric charges of a $M^{2+}{}_2Al$-LDH matrix by three Fol^{3-} and one Cl^- ions, respecting the 10 × 0.25 nm^2 of the inorganic surface area and the projected area of 1.1 nm^2 of each folate ion on the layers. Considering this proportion between positive and negative charges, Figure S3b shows a possible stacking arrangement of the layers. Although the numerical values were estimated to the suggestions presented in Figure S3, the chemical analysis reported ahead to Zn_2Al-Fol-S,F and Mg_2Al-Fol-F,S corroborated to a Fol^{3-}:Cl^- molar proportion equal to 3:1. Co-intercalation was also previously observed for robust anions with a small charge, such as sulindac[26] and pravastatin.[27]

Comparing the slow and fast coprecipitation approach, materials obtained in this work presented higher crystallinity when obtained by the former method, as noticed by the better resolution, higher intensity, and lower width of the 00*l* diffraction peaks (Figures 2a and 2b). Broadening of diffraction peaks is expected for materials possessing small crystallite sizes (mathematically represented for the Scherrer equation),[34,35] as expected for the ones obtained by fast coprecipitation.[35] In addition, taking Zn_2Al-HFol-F as a model, the thermal treatment (at 60 °C for 24 h) did not significantly improve the crystallinity of the material compared to the material without thermal treatment (Figure S4a). However, an additional step of hydrothermal treatment at 150 °C for 1 h improved the crystallinity of Zn_2Al-HFol-F, as noticed in Figure S4b. Ostwald ripening mechanism is anticipated upon hydrothermal treatment, i.e., smaller particles getting dissolved and precipitating into bigger crystals to give more abundant and better-crystalized materials.[36] The XRD patterns (Figure S4b) showed at least five harmonic reflection peaks, indicating a high organization of the stacked LDH layers promoted by the hydrothermal process without producing side phases as zinc oxide.

Vibrational spectroscopy

Vibrational spectroscopy can be applied to confirm the presence of folate species in the LDH samples since distinct anions (H_2Fol^- and Fol^{3-}) are expected according to the pH value of the synthesis. The FTIR and FT-Raman (Figures 3a and 3b) results were analyzed according to our previous work,[37] in which sodium folate salts (Na_2HFol and Na_3Fol) were taken as a reference of di- and trivalent anions, and DFT calculations supported the interpretation of the results. The intercalation of $HFol^{2-}$ was confirmed in Zn_2Al-HFol-S and Zn_2Al-HFol-F because: (*i*) the band at 1690 cm^{-1} region, attributed to νCα,β=O from glutamic acid moiety (with contribution from νC4=O), was much

lower in comparison to FA, as reported previously;[37] (*ii*) two bands were observed in the 1550-1500 and 1400 cm^{-1} spectral region, which are attributed to antisymmetric (ν_{as}) and symmetric stretching (ν_s) vibration of carboxylate groups (COO^-) from glutamate, respectively; (*iii*) no indication of deprotonated PT group was observed. The Fol^{3-} species are characterized by the band at 1500 cm^{-1} region ($\nu C(4)–O^-$ and $\nu_{as}C\alpha'OO^-$) being more intense than the band at 1600 cm^{-1} (benzene stretching). Furthermore, while the Raman spectrum of $HFol^{2-}$ presented splinted bands at 1330 and 1300 cm^{-1} region (also in IR spectra), Fol^{3-} presented overlapped bands around 1340 cm^{-1}, which is attributed to the increase in the aromaticity of rings in PT moiety due to the deprotonation of N3–H group. Such spectral profile was only observed for Mg_2Al-Fol-S (Figure 3a) and Mg_2Al-Fol-F and Zn_2Al-Fol-F (Figure 3b), confirming the presence of Fol^{3-} in such materials. Although Zn_2Al-Fol-S presented a vibrational profile like Zn_2Al-HFol-S (Figure 3a), its spectrum also presented overlapped bands around 1340 cm^{-1} (in Raman and IR spectra) characteristic of Fol^{3-} species. These results suggested the intercalation of both $HFol^{2-}/Fol^{3-}$, attributed to the pH 9.0 applied in synthesizing such samples. The materials prepared by the ion-exchange method presented FTIR's spectral profile of intercalated $HFol^{2-}$ with the contribution of vibrational bands of NO_3^- anion (Figure S2b).

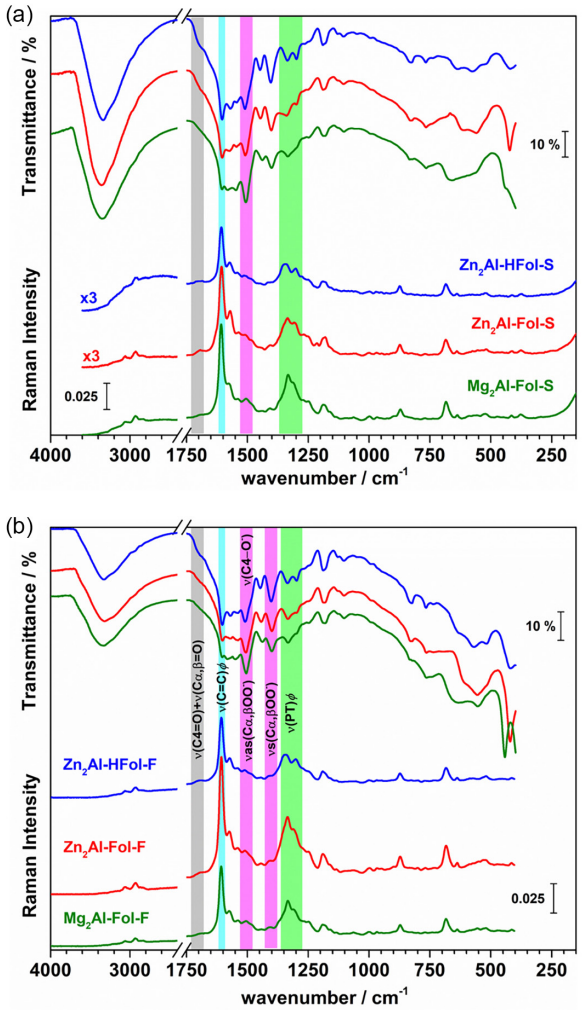

Figure 3. FTIR (ATR) (top) and FT-Raman (bottom) spectra of samples obtained by slow coprecipitation (a) and by fast coprecipitation (b).

Vibrational spectroscopy results indicated that the organic anions did not decompose during the synthesis, keeping their chemical identities, even when submitted to hydrothermal treatment (Figure S5, SI section). In addition, the position of the band of LDH-FA regarding the carboxylate and PT groups presented values close to the sodium salts reported previously,[37] which suggests a coulombic interaction between guest and host.[38]

The strong broadband in the 2800-3600 cm^{-1} region can be attributed to O–H stretching from M–OH groups of LDH layers and hydration water molecules.[39] A signal around 1650 cm^{-1} is assigned to the bending vibration of hydration water.[39] The bands below 1000 cm^{-1} have the contribution of M–OH and M–O vibrations.[39] Such bands were not resolved in the FT-Raman spectra of LDH-FA because the cross-section of the LDH layer is not as high as that of the organic anion.[40]

Electron microscopy

SEM micrographs of representative samples Zn_2Al-HFol-S, Zn_2Al-Fol-S and Mg_2Al-Fol-S are compared in Figure 4. In general, the Mg_2Al-Fol-S presented aggregated particles with flake-type (considerable length and small thickness) morphology, while the particles of Zn_2Al-HFol-S material were much smaller without a

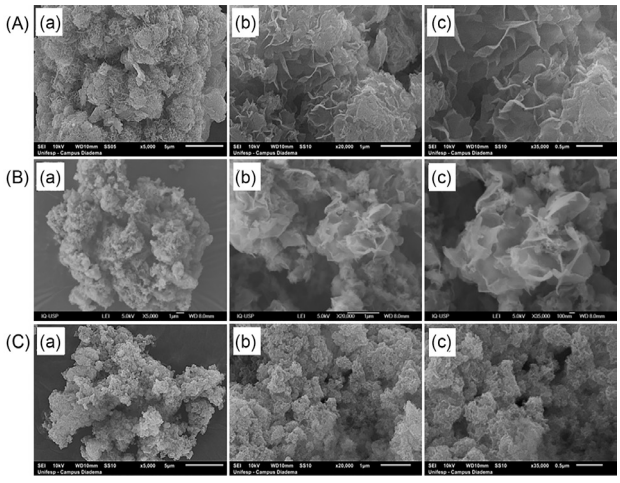

Figure 4. SEM micrographs of representative samples (A) Mg_2Al-Fol-S, (B) Zn_2Al-Fol-S and (C) Zn_2Al-HFol-S obtained by slow coprecipitation; magnified 5,000× (a), 20,000× (b) and 50,000× (c).

defined morphology. The Zn_2Al-Fol-S and Mg_2Al-Fol-S materials presented similar sizes and morphologies. The materials intercalated with Fol^{3-} (synthesized at pH above 9.0) seemed a particle growth favored in the *a/b* plane. Therefore, the results indicated that the morphology of LDH-FA was driven by the protonation level of folate anion instead of the layer's chemical composition.

Figure 5 shows the TEM images of samples prepared by slow (Mg_2Al-Fol-S and Zn_2Al-HFol-S) and fast (Mg_2Al-Fol-F and Zn_2Al-HFol-F) methods for comparison. In general, materials presented aggregates of particles with distinct shapes. The results showed that materials intercalated with Fol^{3-} had larger diameter particles than the ones intercalated with $HFol^{2-}$ (see Figures 5c, 5d and S6, SI section), in line with what was noticed by SEM analysis (Figure 4). The particle size of samples obtained by the fast coprecipitation method was smaller than that obtained by the slow addition of reactants to the folate solution (conventional method). These results agreed with Zhao *et al.*[35] for the Mg/Al-CO_3 counterpart. According to the authors, in the slow addition approach, the particle nucleation and growth steps occur concomitantly because the nuclei formed at the beginning have a long time to grow until the end of the synthetic process. For instance, such results are valuable in the context of drug delivery since LDH particle size influences the pharmacokinetics and pharmacodynamics of the system.[14,41,42] Large particles can decrease drug release rates due to a longer diffusion path than the small ones.[41] Besides, LDH particles less than 20 nm can reach the cellular nucleus while those up to 180 nm stay in the cytoplasm.[42]

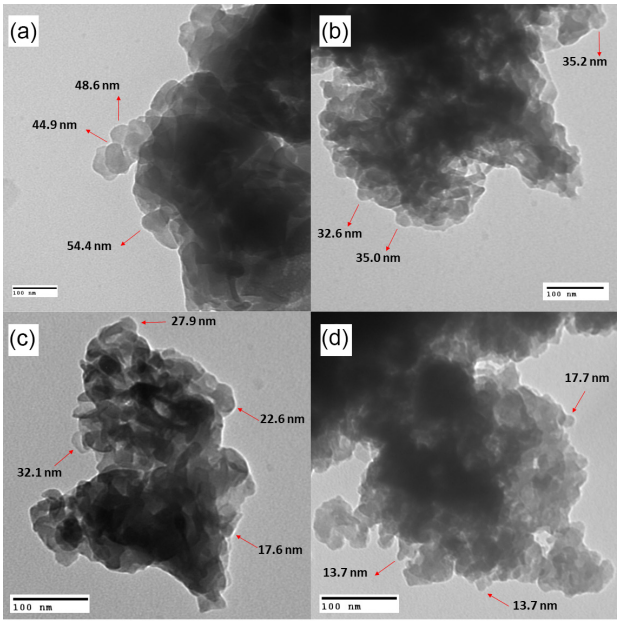

Figure 5. TEM micrographs of samples Mg_2Al-Fol-S (a) and Zn_2Al-HFol-S (b) obtained by slow coprecipitation and samples Mg_2Al-Fol-F (c) and Zn_2Al-HFol-F (d) obtained by fast coprecipitation. Red arrows indicate the estimated diameter of the particles.

Thermal analysis (TGA-DSC and DTG-MS)

Thermal analysis data are presented in Figure 6 and summarized in Table S5 (SI section). Endothermic events (DSC curves) and water release (*m/z* 18; MS curves) indicated the dehydration of samples up to 184 and 242 °C for Zn_2Al-LDH and Mg_2Al-LDH materials, respectively. Under the experimental conditions used in this work, the dehydroxylation of Zn_2Al-LDH materials occurred around the 150-300 °C range, as noticed by endothermic events (DSC curves) and water release (*m/z* 18; MS curves). On the other hand, the dehydroxylation of Mg_2Al-LDH samples initiated above 220 °C and was concurrent with the first thermal oxidation event of folate anions. As reported in the literature,[26,43] Zn_2Al-LDH hydroxide layers are less thermal stable than the Mg_2Al-LDH ones.

The intercalation improved the thermal stability of anionic species compared with pristine FA, but the data were close to those observed for Na_2HFol and Na_3Fol salts.[37] Taking into account the beginning of CO_2 release (*m/z* 44; MS curves) associated with exothermic events (DSC curve) and comparing with our previously reported results for FA and folate sodium salts, the following stability order could be established: Zn_2Al-Fol-F (315 °C) > Na_3Fol (300 °C) ca. Mg_2Al-Fol-S (297 °C) > Zn_2Al-HFol-F (294 °C) ca. Zn_2Al-HFol-S (290 °C) ≥ Mg_2Al-Fol-F (288 °C) ca. Zn_2Al-Fol-S (285 °C) > Na_2HFol (267 °C) > FA (198 °C). Besides, the thermal behavior of intercalated anions was distinct when Zn_2Al-HFol, Zn_2Al-Fol and Mg_2Al-Fol materials obtained from fast and slow methods were compared. The changes in the thermal behavior depend on the nature of the anion[37] (folate speciation, Figure S1), its arrangement between the layers (Figure 2), and the composition of the LDH layer (zinc or magnesium in this work).[26] These parameters influence the interactions between guest-host, guest-water and guest-guest.

After the dehydration step, materials prepared by the fast coprecipitation method presented, in general, more defined thermal events attributed to the oxidation of folate anions (TGA-DSC and DTG-MS curves; Figure 6). Such differences can be attributed to the smaller particle size of the samples obtained through the fast approach. Typically, an advancement in thermal events is experimentally observed for materials that exhibit small particles, although the underlying reasons are not fully understood.[44] One plausible explanation is that thermal conduction is higher for smaller particles than for larger ones.[44,45] Taking Mg_2Al-Fol-S,F as examples, the oxidation events of folate anions occurred at

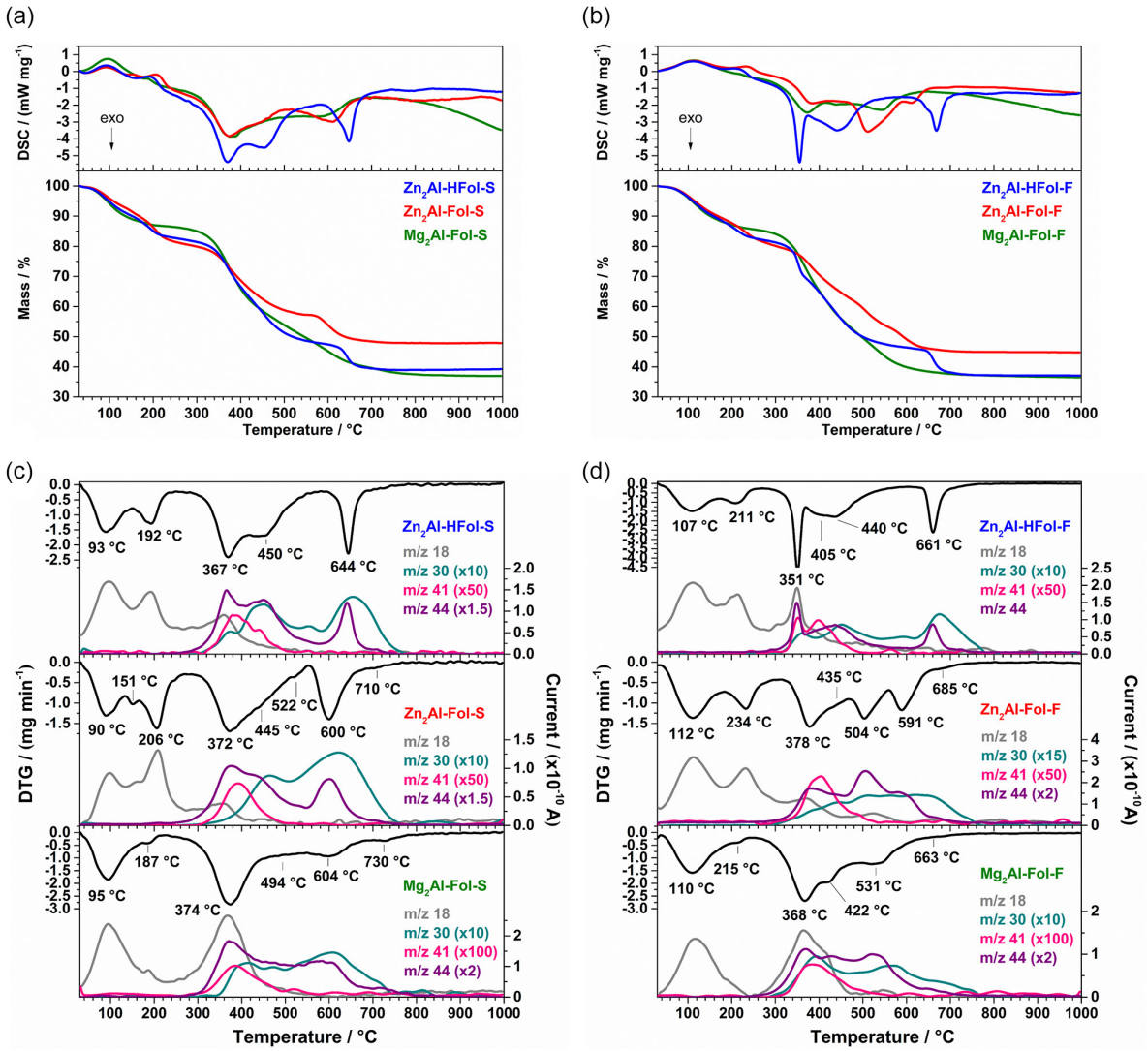

Figure 6. TG-DSC (a,b) and DTG-MS (c,d) curves of samples obtained by slow coprecipitation (a,c) and fast coprecipitation (b,d).

higher temperature values (see DTG peaks) for Mg_2Al-Fol-S than Mg_2Al-Fol-F (Figures 6c and 6d). On the other hand, marked differences in the thermal oxidative events were observed for Zn_2Al-Fol counterparts, especially in the 450-550 °C range. It could be associated with the distinct thermal behavior of $HFol^{2-}$ and Fol^{3-} anions;[37] since $HFol^{2-}/Fol^{3-}$ species were co-intercalation into Zn_2Al-Fol-S material, as indicated by vibrational data, while only Fol^{3-} was expected in Zn_2Al-Fol-F.

Chemical elemental analysis

The chemical elemental analysis data are presented in Table 1, and the results indicated that the material layers had an M^{2+}/Al^{3+} ($M^{2+} = Mg^{2+}$ and Zn^{2+}) molar ratio close to the nominal value (i.e., 2). However, this value was lower than expected for Zn_2Al-HFol. The complexing character of folic acid (folate) against transition metals[46] could explain such results. The same was not observed for LDH-Cl materials synthesized by a similar method, as reported in the literature,[26] evidencing the role of the organic anion in zinc precipitation. The formation of [Zn(FA)] and $[Zn(FA)_2]$ complexes is expected in slightly neutral media, and their global stability constants, expressed as log K, are −1.34 and 4.37, respectively.[47] One can consider that during the synthesis of LDH-FA, both intercalation and complexation reactions occur concomitantly in the conditions used in this work for Zn_2Al-HFol-S. Tronto *et al.*[48] studied the synthesis of Mg_2Al-LDH intercalated with citrate anions and proposed that only the complexation reaction occurs at the beginning of precursors addition into the anion solution. As the addition progresses and the coprecipitation starts, the equilibrium is displaced to the intercalation reaction. Complementary, the higher $[Zn^{2+}]/[Al^{3+}]$ molar ratio determined for Zn_2Al-Fol-S than for Zn_2Al-HFol-S

Table 1. Chemical composition and proposed formula for LDH-FA materials

Proposed formula	M^{2+}/Al^{3+a}	H_2O^b / wt.%	C^c / wt.%	N^c / wt.%	$Rm^{b,d}$ / wt.%	LC^e / %
Zn_2Al-HFol-S $[Zn_{1.72}Al(OH)_{5.44}](C_{19}H_{17}O_6N_7^{2-})_{0.5}{\cdot}2.52H_2O$	1.72 ± 0.02 (1.72)	9.8 (10.0)	22.8 ± 0.04 (22.7)	9.62 ± 0.10 (9.77)	39.3 (38.1)	43.8
Zn_2Al-Fol-S $[Zn_{1.90}Al(OH)_{5.80}](C_{19}H_{16}O_6N_7^{3-})_{0.27}(C_{19}H_{17}O_6N_7^{2-})_{0.05}Cl^-_{0.09}{\cdot}2.32H_2O$	1.90 ± 0.02 (1.90)	9.7 (9.6)	16.7 ± 0.09 (16.8)	7.21 ± 0.01 (7.21)	47.9 (47.3)	32.2
Mg_2Al-Fol-S $[Mg_{2.21}Al(OH)_{6.42}](C_{19}H_{16}O_6N_7^{3-})_{0.30}Cl^-_{0.10}{\cdot}2.70H_2O$	2.21 ± 0.07 (2.21)	13.2 (13.0)	18.8 ± 0.12 (18.3)	7.81 ± 0.04 (7.88)	37.0 (37.5)	35.2
Zn_2Al-HFol-F $[Zn_{1.97}Al(OH)_{5.94}](C_{19}H_{17}O_6N_7^{2-})_{0.50}{\cdot}3.45H_2O$ + (ads. $Na_2HFol)_{0.11}$	1.97 ± 0.01 (1.97)	10.9 (10.5)	23.5 ± 0.06 (23.5)	10.3 ± 0.01 (10.1)	37.1 (36.8)	45.3
Zn_2Al-Fol-F $[Zn_{1.97}Al(OH)_{5.94}](C_{19}H_{16}O_6N_7^{3-})_{0.30}Cl^-_{0.10}{\cdot}2.94H_2O$ + (ads. $Na_3Fol)_{0.08}$	1.97 ± 0.02 (1.97)	11.1 (10.9)	17.9 ± 0.07 (17.9)	7.71 ± 0.04 (7.67)	44.8 (45.1)	34.3
Mg_2Al-Fol-F $[Mg_{2.17}Al(OH)_{6.34}](C_{19}H_{16}O_6N_7^{3-})_{0.30}Cl^-_{0.10}{\cdot}2.92H_2O$	2.17 ± 0.00 (2.17)	14.2 (14.0)	18.3 ± 0.01 (18.3)	7.85 ± 0.02 (7.84)	36.5 (36.9)	35.1

[a]Measured by inductively coupled plasma optical emission spectroscopy (ICP OES) (M^{2+}: Mg^{2+} or Zn^{2+}); [b]measured by thermal analysis under air atmosphere; [c]measured by carbon, hydrogen and nitrogen analysis; [d]Rm refers to residual mass from thermal analysis results; [e]LC is the loading capacity calculated by the formula: LC (%) = [An-/LDH-An- weight] × 100. The values in parentheses indicate theoretical results calculated from proposed formulas.

(Table 1) indicated that the increase of pH (more OH^- ions are available and Zn-FA complexation is precluded) could favor the formation of Zn_2Al-LDH phase. It must also be considered that the complexation reaction can also be prevented by lowering the [FA]/[Al^{3+}] molar ratio, leading to the Zn^{2+} increasing content in the intralayer, as previously noticed for Zn_2Al-LDH intercalated with the ciprofloxacin anion.[49] No difference between the nominal and the experimental Zn^{2+} content was observed (Table 1) for Zn_2Al-HFol-F and Zn_2Al-Fol-F materials synthesized by fast coprecipitation ([FA]/[Al^{3+}] = 0.67).

The elemental analysis results agreed with the co-intercalation of $HFol^{2-}/Fol^{3-}$ in Zn_2Al-Fol-S, which aligns with the vibrational spectroscopy analysis. According to the FA speciation curves (Figure S1), in the synthesis pH value of 9.0, the molar fractions of divalent ($HFol^{2-}$) and trivalent (Fol^{3-}) folate anions in solution are expected to be around 0.1 and 0.9, respectively. However, chemical speciation can differ considering the synthesis medium containing Zn^{2+}, Al^{3+}, OH^- anions, and LDH suspended particles. In addition, to match the proposal formulas considering the carbon and nitrogen percentages, the presence of small amounts of adsorbed Na_2Hfol and Na_3Fol in the Zn_2Al-HFol-F and Zn_2Al-Fol-F materials, respectively, was suggested. The washing steps probably did not surpass the interaction between the organic anions on the LDH external surface. The hydrothermal treatment of the Zn_2Al-HFol-F sample led to the leaching of only around 1.8% of Zn^{2+}. For Mg_2Al-Fol-S and Mg_2Al-Fol-F, the proposed chemical formulas were similar, indicating that variations did not influence the Mg_2Al-LDH phase in the synthesis parameters. Moreover, the elemental analysis results for materials synthesized at pH above 9.0 also suggested the co-intercalation of Fol^{3-}/Cl^- in a 3:1 ratio (Table 1), as proposed by XRD analysis (Figure S3).

The loading capacity of LDH-FA materials synthesized in this work (Table 1) was higher or as high as those reported in the literature (indicated in Table S1). The chemical elemental analysis results agreed with thermal analysis (considering the residual mass), XRD and spectroscopic (IR and Raman) data. In addition, it is worth highlighting that the synthesis of LDH/organic anion hybrid materials obtained by fast coprecipitation has yet to be explored in the literature. For the first time, such a synthesis approach was applied to prepare Zn_2Al-HFol-F, Zn_2Al-Fol-F and Mg_2Al-Fol-F materials, with high synthesis yields of 77, 79 and 82%, respectively.

Conclusions

In this work, M^{2+}/Al^{3+}-LDH (M^{2+} = Mg^{2+} or Zn^{2+}) materials intercalated with folate anions ($HFol^{2-}$ or Fol^{3-}) were synthesized and characterized by a set of physicochemical techniques going further than what has already been reported in the literature. Two synthetic approaches (i.e., slow and fast coprecipitation) were applied to obtain materials with phase purity and high loading capacity. The pH of synthesis media drove the protonation level of intercalated folate species, which was attributed to the FA speciation in the pH range of work, confirmed by vibrational spectroscopy and chemical analysis. Consequently, the arrangement of the folates in the interlayer region of LDH (XRD analysis), as well as the size of the material's particles (SEM and TEM), their loading capacity (chemical analysis) and thermal behavior (TGA/DTG-DSC-MS)

were dependent of the coprecipitation pH value. Comparing the synthetic approaches, the main difference observed was the lesser crystallinity degree and particle diameter of materials obtained by fast coprecipitation. This detailed work could contribute to the subsequent research concerning the application of LDH intercalated with folate anions or other anions from polyprotic organic acids.

Supplementary Information

Supplementary data are available free of charge at http://jbcs.sbq.org.br as a PDF file.

Acknowledgments

V. R. M. is grateful to the Coordenação de Aperfeiçoamento de Pessoal de Nível Superior (CAPES, Brazil, Finance Code 33002010191P0) for the PhD scholarship. C. S. M. acknowledges the Fundação de Amparo à Pesquisa do Estado de São Paulo for a research grant (FAPESP 12/06291-4). V. R. L. C. is thankful to the Conselho Nacional de Desenvolvimento Científico e Tecnológico (CNPq, 314034/2021-8) and FAPESP (INCT-INEO 2014/50869-6) for the research grants. This work was partially supported by the region Auvergne-Rhone Alpes (Pack Ambition International AURA program). The authors are thankful to the Laboratório de Cristalografia (Instituto de Física-USP) for the XRD diffractograms registration, the Laboratório de Espectroscopia Molecular (LEM, Instituto de Química-USP) for the Raman and FTIR spectra, and Prof Marcos A. Bizeto (Universidade Federal de São Paulo-UNIFESP, Campus Diadema-SP) for the SEM analysis.

Author Contributions

Vagner R. Magri was responsible for conceptualization, visualization, investigation, synthesis methodology, formal analysis, data curation, writing the original draft, and reviewing, and editing; Caroline S. de Matos and Michele A. Rocha for synthesis methodology, writing, review, and editing; Christine Taviot-Gueho for formal analysis, funding acquisition and writing, review, and editing; Vera R. L. Constantino for conceptualization, visualization, investigation, project management, supervision, funding acquisition, synthesis methodology, writing, review, and editing.

References

1. Constantino, V. R. L.; Figueiredo, M. P.; Magri, V. R.; Eulálio, D.; Cunha, V. R. R.; Alcântara, A. C. S.; Perotti, G. F.; *Pharmaceutics* **2023**, *15*, 413. [Crossref]
2. Saha, S.; Ray, S.; Acharya, R.; Chatterjee, T. K.; Chakraborty, J.; *Appl. Clay Sci.* **2017**, *135*, 493. [Crossref]
3. Cao, Z.; Li, B.; Sun, L.; Li, L.; Xu, Z. P.; Gu, Z.; *Small Methods* **2020**, *4*, 1900343. [Crossref]
4. Cunha, V. R. R.; Ferreira, A. M. C.; Constantino, V. R. L.; Tronto, J.; Valim, J. B.; *Quim. Nova* **2010**, *33*, 159. [Crossref]
5. Constantino, V. R. L.; Cunha, V. R. R.; Rocha, M. A.; Figueiredo, M. P.; Magri, V. R.; Eulálio, D.; Perotti, G. F.; Bizeto, M. A.; Zambuzzi, W. F.; Koh, I. H. J. In *Progress in Layered Double Hydroxides: From Synthesis to New Applications*, vol. 8; Nocchetti, M.; Costantino, U., eds.; World Scientific: Singapore, 2022, p. 413-482.
6. Cavani, F.; Trifirò, F.; Vaccari, A.; *Catal. Today* **1991**, *11*, 173. [Crossref]
7. Rives, V.; *Layered Double Hydroxides: Present and Future*; Rives, V.; Nova Science Publishers, Inc.: New York, 2001.
8. Ducker, G. S.; Rabinowitz, J. D.; *Cell Metab.* **2017**, *25*, 27. [Crossref]
9. Jones, P.; Lucock, M.; Scarlett, C. J.; Veysey, M.; Beckett, E. L.; *J. Nutr. Intermed. Metab.* **2019**, *18*, 100104. [Crossref]
10. Saini, R. K.; Nile, S. H.; Keum, Y.; *Food Res. Int.* **2016**, *89*, 1. [Crossref]
11. Kancherla, V.; Wagh, K.; Johnson, Q.; Oakley, G. P.; *Birth Defects Res.* **2018**, *110*, 1139. [Crossref]
12. Scaranti, M.; Cojocaru, E.; Banerjee, S.; Banerji, U.; *Nat. Rev. Clin. Oncol.* **2020**, *17*, 349. [Crossref]
13. Nogueira, E.; Gomes, A. C.; Preto, A.; Cavaco-Paulo, A.; *Nanomed. Nanotechnol., Biol. Med.* **2016**, *12*, 1113. [Crossref]
14. Oh, J. M.; Choi, S. J.; Lee, G. E.; Kim, J. E.; Choy, J. H.; *Chem. - Asian J.* **2009**, *4*, 67. [Crossref]
15. Park, D.-H.; Cho, J.; Kwon, O.-J.; Yun, C.-O.; Choy, J.-H.; *Angew. Chem., Int. Ed.* **2016**, *55*, 4582. [Crossref]
16. Qin, L.; Wang, S.; Zhang, R.; Zhu, R.; Sun, X.; Yao, S.; *J. Phys. Chem. Solids* **2008**, *69*, 2779. [Crossref]
17. Xiao, R.; Wang, W.; Pan, L.; Zhu, R.; Yu, Y.; Li, H.; Liu, H.; Wang, S.-L.; *J. Mater. Sci.* **2011**, *46*, 2635. [Crossref]
18. Qin, L.; Wang, W.; You, S.; Dong, J.; Zhou, Y.; Wang, J.; *Int. J. Nanomed.* **2014**, *9*, 5701. [Crossref]
19. Kim, T.-H.; Oh, J.-M.; *J. Solid State Chem.* **2016**, *233*, 125. [Crossref]
20. Arízaga, G. G. C.; Jiménez, C. S.; Saavedra, K. J. P.; Lamas, A. M. M.; Pérez, A. M. P.; *Micro Nano Lett.* **2016**, *11*, 360. [Crossref]
21. Mallakpour, S.; Hatami, M.; *Int. J. Biol. Macromol.* **2019**, *122*, 157. [Crossref]
22. Pagano, C.; Perioli, L.; Latterini, L.; Nocchetti, M.; Ceccarini, M. R.; Marani, M.; Ramella, D.; Ricci, M.; *Appl. Clay Sci.* **2019**, *168*, 382. [Crossref]
23. Arratia-Quijada, J.; Sánchez Jiménez, C.; Gurinov, A.; Pérez Centeno, A.; Ceja Andrade, I.; Carbajal Arízaga, G. G.; *Mater. Sci. Eng., B* **2016**, *203*, 7. [Crossref]

24. Szakács, Z.; Noszál, B.; *Electrophoresis* **2006**, *27*, 3399. [Crossref]
25. Cunha, V. R. R.; Petersen, P. A. D.; Souza, R. B.; Martins, A. M. C. R. P. F.; Leroux, F.; Taviot-Gueho, C.; Petrilli, H. M.; Koh, I. H. J.; Constantino, V. R. L.; *New J. Chem.* **2020**, *44*, 10011. [Crossref]
26. Rocha, M. A.; Petersen, P. A. D.; Teixeira-Neto, E.; Petrilli, H. M.; Leroux, F.; Taviot-Gueho, C.; Constantino, V. R. L.; *RSC Adv.* **2016**, *6*, 16419. [Crossref]
27. Cunha, V. R. R.; Petersen, P. A. D.; Gonçalves, M. B.; Petrilli, H. M.; Taviot-Gueho, C.; Leroux, F.; Temperini, M. L. A.; Constantino, V. R. L.; *Chem. Mater.* **2012**, *24*, 1415. [Crossref]
28. Rubenstein, M.; *Chem3D Pro*, version 12.0.2; Harvard University, USA, 2010.
29. Kaduk, J. A.; Crowder, C. E.; Zhong, K.; *Powder Diffr.* **2015**, *30*, 52. [Crossref]
30. Figueiredo, M. P.; Cunha, V. R. R.; Cellier, J.; Taviot-Gueho, C.; Constantino, V. R. L.; *ChemistrySelect* **2022**, *7*, e202103880. [Crossref]
31. Gocheva, G.; Petkov, N.; Garcia Luri, A.; Iliev, S.; Ivanova, N.; Petrova, J.; Mitrev, Y.; Madjarova, G.; Ivanova, A.; *J. Mol. Liq.* **2019**, *292*, 111392. [Crossref]
32. Cunha, V. R. R.; Guilherme, V. A.; de Paula, E.; de Araujo, D. R.; Silva, R. O.; Medeiros, J. V. R.; Leite, J. R. S. A.; Petersen, P. A. D.; Foldvari, M.; Petrilli, H. M.; Constantino, V. R. L.; *Mater. Sci. Eng. C* **2016**, *58*, 629. [Crossref]
33. Costantino, U.; Coletti, N.; Nocchetti, M.; Aloisi, G. G.; Elisei, F.; *Langmuir* **1999**, *15*, 4454. [Crossref]
34. Valente, J. S.; Lima, E.; Toledo-Antonio, J. A.; Cortes-Jacome, M. A.; Lartundo-Rojas, L.; Montiel, R.; Prince, J.; *J. Phys. Chem. C* **2010**, *114*, 2089. [Crossref]
35. Zhao, Y.; Li, F.; Zhang, R.; Evans, D. G.; Duan, X.; *Chem. Mater.* **2002**, *14*, 4286. [Crossref]
36. Sun, X.; Neuperger, E.; Dey, S. K.; *J. Colloid Interface Sci.* **2015**, *459*, 264. [Crossref]
37. Magri, V. R.; Rocha, M. A.; de Matos, C. S.; Petersen, P. A. D.; Leroux, F.; Petrilli, H. M.; Constantino, V. R. L.; *Spectrochim. Acta, Part A* **2022**, *273*, 120981. [Crossref]
38. Nara, M.; Torii, H.; Tasumi, M.; *J. Phys. Chem.* **1996**, *100*, 19812. [Crossref]
39. Kloprogge, J. T.; Hickey, L.; Frost, R. L.; *J. Raman Spectrosc.* **2004**, *35*, 967. [Crossref]
40. Gil, O. M.; Rocha, M. A.; Constantino, V. R. L.; Koh, I. H. J.; de Faria, D. L. A.; *Vib. Spectrosc.* **2016**, *87*, 60. [Crossref]
41. Gu, Z.; Wu, A.; Li, L.; Xu, Z.; *Pharmaceutics* **2014**, *6*, 235. [Crossref]
42. Li, S.; Li, J.; Wang, C. J.; Wang, Q.; Cader, M. Z.; Lu, J.; Evans, D. G.; Duan, X.; O'Hare, D.; *J. Mater. Chem. B* **2013**, *1*, 61. [Crossref]
43. Frost, R. L.; Martens, W.; Ding, Z.; Kloprogge, J. T.; *J. Therm. Anal. Calorim.* **2003**, *71*, 429. [Crossref]
44. Ionashiro, M.; *Giolito: Princípios Básicos da Termogravimetria e Análise Térmica Diferencial/ Calorimetria Exploratória Diferencial*; GIZ Editorial: São Paulo, 2004.
45. Hu, S.; Li, W.; *ChemCatChem* **2018**, *10*, 2900. [Crossref]
46. El-Wahed, M. G. A.; Refat, M. S.; El-Megharbel, S. M.; *Spectrochim. Acta, Part A* **2008**, *70*, 916. [Crossref]
47. Fazary, A. E.; Ramadan, A. M.; *Complex Met.* **2014**, *1*, 139. [Crossref]
48. Tronto, J.; Crepaldi, E. L.; Pavan, P. C.; Cipriano De Paula, C.; Valim, J. B.; *Mol. Cryst. Liq. Cryst.* **2001**, *356*, 227. [Crossref]
49. Cherif, N. F.; Constantino, V. R. L.; Hamdaoui, O.; Leroux, F.; Taviot-Guého, C.; *New J. Chem.* **2020**, *44*, 10076. [Crossref]

Submitted: February 23, 2024
Published online: July 11, 2024